Hindered rotation in ion-neutral molecular complexes: The ν_1 vibration of $H_2–HCO^+$ and $D_2–DCO^+$

Rouslan V. Olkhov, Sergey A. Nizkorodov, and Otto Dopfer[a)]

Institut für Physikalische Chemie, Universität Basel, Klingelbergstrasse 80, CH-4056 Basel, Switzerland

Infrared spectra of the mass selected ionic complexes $H_2–HCO^+$ and $D_2–DCO^+$ have been recorded in the vicinity of their ν_1 vibrations (H_2/D_2 stretch) by means of photofragmentation spectroscopy. The anomalous rotational constants obtained by fitting the observed line positions to a semirigid Watson A-type Hamiltonian reflect the appreciable zero-point excursions of the H_2/D_2 molecule. Barriers for this internal motion are estimated utilizing a simple atom–diatom hindered rotor Hamiltonian. According to this one-dimensional model, the barrier increases by about 15% upon vibrational excitation which is mainly attributed to electrostatic effects. © *1997 American Institute of Physics.* [S0021-9606(97)00344-9]

I. INTRODUCTION

In the last decade photodissociation spectroscopy of mass selected ionic complexes[1–6] has been demonstrated to be a sensitive and selective technique for the investigation of the intermolecular interactions in charged systems. In contrast to their neutral counterparts,[7,8] ionic complexes are spectroscopically far less well characterized.[3,9] In our laboratory the focus has recently been placed on IR predissociation spectroscopy of proton-bound complexes.[10–13] Rotationally resolved spectra of dimers have revealed useful information about their intermolecular potentials, while vibrational spectra have elucidated microsolvation phenomena in larger clusters. The present paper extends a previous spectroscopic and theoretical study[10] on the T-shaped proton-bound $H_2–HCO^+$ dimer, a stable isomer of protonated formaldehyde. This complex represents the stabilized intermediate of the astrophysically important exothermic proton transfer reaction $H_3^+ + CO \rightarrow H_2 + HCO^+$. In contrast to the recently studied $Rg–HCO^+$ complexes ($Rg=He$, Ne, Ar),[11–13] $H_2–HCO^+$ features an additional possibility of hindered internal rotation of the hydrogen moiety.[10]

In the past, high resolution spectroscopic techniques have proven to be useful tools for extracting structural properties of rigid molecules from the measured rotational constants. However, for floppy systems with shallow potential minima and hence largely delocalized vibrational wave functions, the conversion of spectroscopic constants into potential energy surface parameters is not trivial. The available spectral data usually probe only limited parts of the potential energy surface. Hence, their interpretation can significantly depend on the Hamiltonian used for the analysis. For example, Nesbitt and Naaman[14] have shown that a low temperature rovibrational spectrum of an atom–diatom complex with a T-shaped equilibrium structure can be reproduced with reasonable accuracy by both a semirigid asymmetric top Hamiltonian and a simple one-dimensional hindered internal rotor model.

In a previous paper,[10] IR predissociation spectra of the $H_2–HCO^+$ complex in the range of $2500–4500 \ cm^{-1}$ have been reported. Two intense intramolecular fundamentals, namely, ν_1 (H_2 stretch, $\approx 4060 \ cm^{-1}$) and ν_2 (CH stretch, $\approx 2840 \ cm^{-1}$), and several weaker combination bands of ν_2 with intermolecular vibrations were observed. The vibrational assignment was guided by *ab initio* calculations at the QCISD(T) level. In agreement with previous computations, the global minimum of the complex was found to be the T-shaped proton-bound geometry (C_{2v}), with a binding energy of $D_e \approx 1440 \ cm^{-1}$ and a barrier for internal H_2 rotation of $V_b \approx 1160 \ cm^{-1}$ via the linear transition state ($C_{\infty v}$). The observed spectrum is consistent with this structure, but not with other isomeric geometries predicted at higher energies on the cluster's potential energy surface, for example, an oxygen-bound T-shaped minimum with $D_e \approx 145 \ cm^{-1}$.

The ν_1 fundamental was the only band for which the rotational structure was not completely washed out by predissociation induced lifetime broadening.[10] Two subbands of this parallel transition have been observed, one of $\Sigma–\Sigma$ type and one of $\Pi–\Pi$ type, corresponding to $K=0–0$ and $1–1$ transitions in the prolate symmetric top limit, respectively. Asymmetry splittings of the $\Pi–\Pi$ subband were not resolved. Therefore, both bands were analyzed separately in terms of a pseudodiatomic Hamiltonian. The resulting constants $\bar{B}=(B+C)/2$ and D indicated that the intermolecular bond is slightly shorter in the Π states (with respect to the corresponding Σ states) and also increases in strength upon ν_1 excitation. Asymmetry splittings, though not resolved, were evident from the J dependent widths of the $\Pi–\Pi$ transition lines. The estimated magnitude of the asymmetry, related to the difference $B–C$, was not consistent with reasonable rigid geometries of the complex. It was, however, shown to be compatible with splittings derived from a simple one-dimensional internal rotor model assuming the calculated *ab initio* potential for the hindered H_2 rotation.[10]

The aim of the present study is to gain a deeper insight into the internal rotation dynamics of the $H_2–HCO^+$ complex. For this purpose, the ν_1 band of the $H_2–HCO^+$ complex has been reinvestigated under improved experimental

---
[a)]Author to whom correspondence should be addressed.

conditions, resulting in spectra with better signal-to-noise ratios and increased spectral resolution. In particular, the asymmetry splittings in the Π–Π transition, which are essential for a more detailed analysis of the internal rotation, could be resolved. Additional information is provided by the corresponding ν_1 spectrum of the isotopic D$_2$–DCO$^+$ complex, because it probes lower lying parts of the hindered rotor potential due to the smaller zero-point energy.

II. EXPERIMENT

Mid-infrared spectra of mass selected H$_2$–HCO$^+$ (D$_2$–DCO$^+$) ionic complexes were recorded by means of photodissociation spectroscopy in a tandem mass spectrometer. The experimental technique and setup have been described in detail previously.[10,13,15] Briefly, the parent complexes were produced in an electron impact ion source by expanding a mixture of CO, H$_2$ (D$_2$), and He with a ratio of about 1:50:50 and a backing pressure of 5 bars through a pulsed nozzle. The first quadrupole mass spectrometer selected the species under study from the variety of ions present in the skimmed supersonic expansion. After passing through a 90° quadrupole deflector the parent ion beam was injected into an octopole ion guide where it was overlapped in space and time with tunable infrared radiation emitted by a pulsed optical parametric oscillator (OPO) laser system with 0.02 cm^{-1} bandwidth. The absorbed photon energy exceeded the binding energy of the cluster ion and eventually induced its dissociation into HCO$^+$ (DCO$^+$) ions and H$_2$ (D$_2$). The second quadrupole transmitted only the fragment ions which were subsequently measured with a Daly detector. Photofragmentation spectra were obtained by monitoring the fragment ion intensity as a function of the photon frequency.

To compensate for any background signals, mainly arising from metastable fragmentation of hot clusters, the ion source was operated at twice the laser frequency (20 Hz), whereby the laser-off signal was subtracted from the laser-on signal. Due to the low transition moment of the ν_1 vibration,[10] the laser-induced dissociation signal of intense lines was, under typical experimental conditions, less than 50% of the one arising from metastable decomposition.

Calibration of the laser frequency was accomplished by recording optoacoustic spectra of C$_2$H$_2$ and HDO utilizing the signal and idler outputs of the OPO system, respectively.[16] Etalon fringes (free spectral range=4 GHz) were simultaneously monitored and improved the accuracy of the calibration compared to the previous study.[10] Line positions were corrected for the Doppler shift caused by the kinetic energy (several eV) of the ions in the octopole. The precision of absolute line positions (<0.02 cm^{-1}) is limited by the uncertainty of the kinetic energy of the ions (±1 eV).

The main experimental improvements compared to the previous work[10] include the installation of an IR power meter used for laser intensity normalization and a more flexible gas inlet system allowing more gas components to be mixed. Substantially higher parent ion currents enabled spectra to be recorded at significantly lower laser power without

a decrease of the signal-to-noise ratio. The reduction of the laser power led to laser limited widths (0.02 cm^{-1}) of the ν_1 rovibrational lines because saturation of the transitions could be avoided. The previously measured linewidth of 0.06 cm^{-1}, mistakenly attributed to lifetime broadening,[10] arose from saturation effects.

III. RESULTS AND DISCUSSION

Figures 1 and 2 show the photofragmentation spectra of H$_2$–HCO$^+$ and D$_2$–DCO$^+$ in the regions of their ν_1 vibrations (H$_2$/D$_2$ stretch). The bands have the rotational structure of a parallel (A-type) transition of a slightly asymmetric prolate top. The small asymmetry is expected from the *ab initio* structure[10] which corresponds to a κ parameter of -0.99986 and -0.99978 for H$_2$–HCO$^+$ and D$_2$–DCO$^+$, respectively. The projection of the total angular momentum J onto the intermolecular axis, K_a, can therefore be considered as a nearly good quantum number.

In the case of H$_2$–HCO$^+$, two subbands are observed corresponding to $K_a=0-0$ ($\Sigma-\Sigma$) and $1-1$ ($\Pi-\Pi$) transitions. The nuclear spin functions of even and odd K_a states have different symmetry corresponding to the *ortho* and *para* modifications of molecular hydrogen. Hence, both Σ and Π states are significantly populated even in a cold beam because spin relaxation rates are usually small.[17] The spectrum shown in Fig. 1 is similar in appearance to the one presented previously.[10] However, in the present study the asymmetry splittings in the P and R branches of the $\Pi-\Pi$ subband are resolved for transitions involving levels with J larger than five (see inset in Fig. 1), allowing for the determination of $B-C$. Furthermore, transitions between higher J levels are observed in the present study, leading to more accurate constants (Table I).

For the D$_2$–DCO$^+$ isotopomer, several transitions of the $\Delta-\Delta$ ($K_a=2-2$) band are identified in addition to lines of the $\Sigma-\Sigma$ and $\Pi-\Pi$ bands (Fig. 2, Table II). Two factors increase the Δ state population of D$_2$–DCO$^+$ compared to H$_2$–HCO$^+$. First, the smaller rotational constant A of D$_2$–DCO$^+$ ($b_{D_2}\approx30$ cm^{-1}, $b_{H_2}\approx60$ cm^{-1})[18] leads to a larger population of higher K_a states for a given temperature. Second, the spin statistical weights favor even K_a states with respect to odd K_a states in the case of D$_2$–DCO$^+$ (2:1), whereas the situation is reversed for H$_2$–HCO$^+$ (1:3).

The unresolved Q branches of the $\Pi-\Pi$ and $\Delta-\Delta$ transitions provide a definitive J assignment in the respective P and R branches. In the case of D$_2$–DCO$^+$, the clear observation of the $P(1)$ and $R(0)$ lines determines the position of the band gap of the $\Sigma-\Sigma$ band. Unfavorable nuclear spin weights for the H$_2$–HCO$^+$ Σ state lead to vanishing line intensities near the $\Sigma-\Sigma$ origin. For this band, the J numbering was prompted by the hindered rotor simulations described below. The band origin determined at 4064.8 cm^{-1} is about $2\bar{B}\approx1$ cm^{-1} larger than the previously reported value[10] of 4063.8 cm^{-1}, reflecting the shift in the J numbering by one unit.

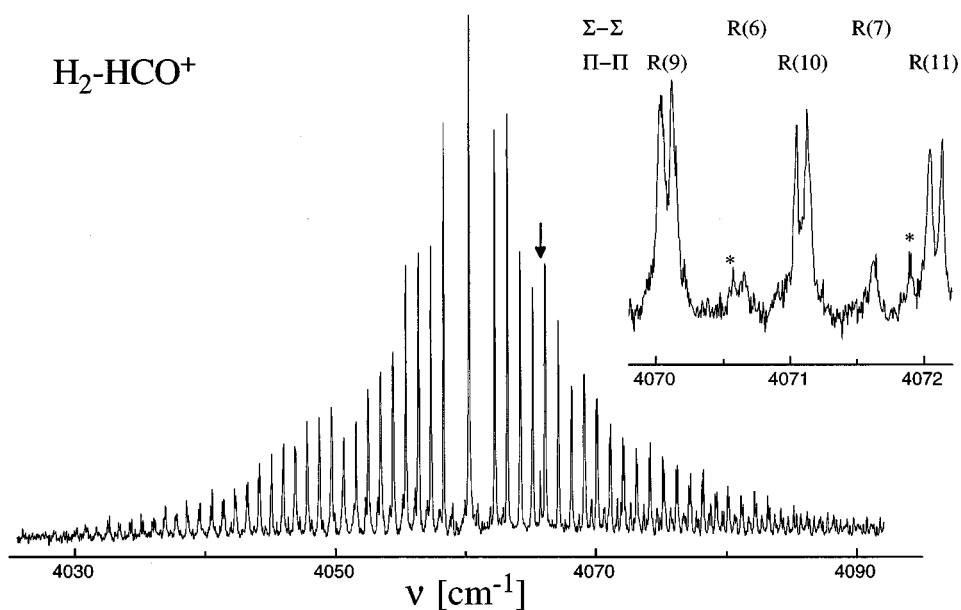In the H$_2$–HCO$^+$ spectrum an additional sharp Q-branch-like feature is observed at about 4065.8 cm^{-1}.

FIG. 1. Infrared photodissociation spectrum of the ν_1 vibration of H_2–HCO^+. The arrow indicates an unassigned Q branch at around 4065.8 cm^{-1}. The inset shows the $R(6)$ and $R(7)$ lines of the Σ–Σ subband, and the $R(9)$–$R(11)$ doublets of the Π–Π subband. Peaks in the inset marked by an asterisk correspond to unassigned lines.

This band is not yet definitively assigned and is probably due to a sequence transition involving ν_1 and either an intermolecular or intramolecular bending vibration. A corresponding band has not been identified in the spectrum of D_2–DCO^+, possibly due to the interference with strong ν_1 band lines. In addition, the H_2–HCO^+ spectrum shows several unassigned

weak series of lines, some of which are marked by an asterisk in the inset of Fig. 1. They are not connected to the above-mentioned Q branch and probably also correspond to various sequence bands.

As mentioned in Sec. I, (at least) two different model Hamiltonians may be used to analyze the observed ν_1 band

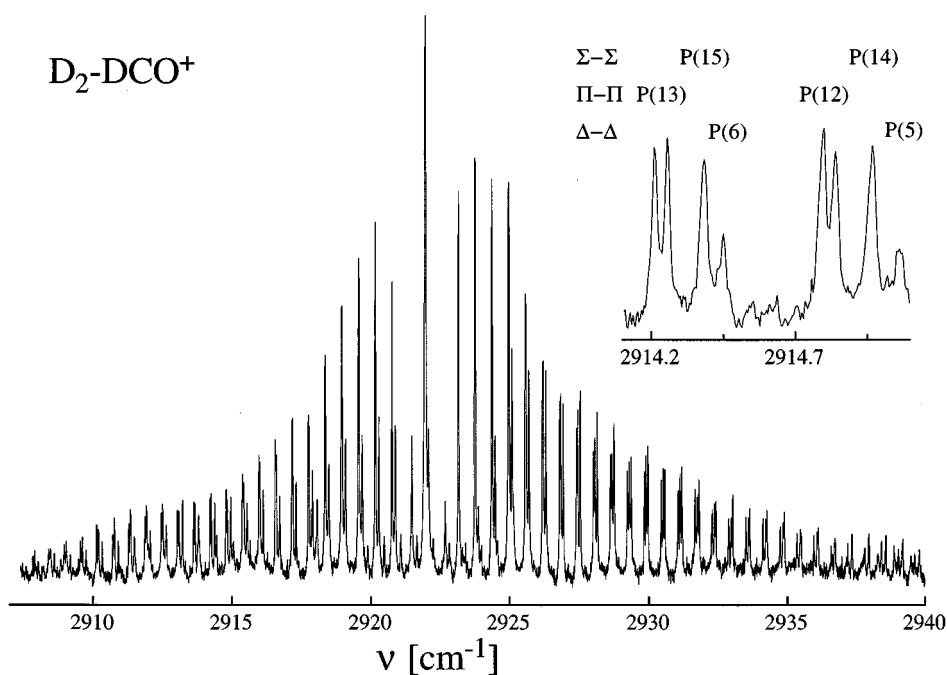FIG. 2. Infrared photodissociation spectrum of the ν_1 vibration of D_2–DCO^+. The inset shows the $P(14)$ and $P(15)$ lines of the Σ–Σ, the $P(12)$ and $P(13)$ doublets of the Π–Π, and the $P(5)$ and $P(6)$ lines of the Δ–Δ subbands.

TABLE I. Rotational constants (in cm^{-1}) obtained for H$_2$–HCO$^+$ by fitting spectral line positions[a] of the ν_1 band to a Watson A-type Hamiltonian.

H$_2$–HCO$^+$	Σ–Σ	Π–Π	Σ–Σ/Π–Π
B''		0.49024(5)	0.48949(8)
C''		0.48399(8)	0.48317(8)
$\bar{B}''$	0.48674(15)	0.48712(5)	0.48633(6)
$D_J'' \times 10^6$	4.0(fixed)	3.5(2.0)	3.66(4)
$D_{JK}'' \times 10^4$			$-10.2(8)$
B'		0.49148(5)	0.49076(8)
C'		0.48514(7)	0.48436(8)
$\bar{B}'$	0.48802(14)	0.48831(4)	0.48756(6)
$D_{J'} \times 10^6$	4.0 (fixed)	3.3(1.9)	3.46(4)
$D_{JK'} \times 10^4$			$-9.8(8)$
$\Delta A = A'' - A'$		4.5296(6)	4.5300(6)
ν_0	4064.8164(34)	4060.2928(6)[b]	4064.8220(6)
R branch	$R(2)$–$R(29)$	$R(1)$–$R(29)$	
P branch	$P(1)$–$P(14)$	$P(2)$–$P(36)$	
Q branch		4060.29(2)	
used lines	42	134	176
rms$\times 10^3$	8.2	6.3	7.0

[a]Available from the authors upon request.
[b]Subband origin is calculated from $\nu_0 - \Delta A$.

spectra: (a) a semirigid asymmetric top Hamiltonian and (b) a one-dimensional hindered rotor Hamiltonian of a floppy molecule. Both strategies will be discussed separately.

A. Semirigid asymmetric top analysis

The degeneracy of each J level in $K_a \neq 0$ manifolds of a prolate symmetric rotor ($B = C$) is removed in an asymmetric prolate top (K-type doubling[19]). For small asymmetry $B - C$, the resulting splitting is proportional to $(B-C)^{K_a}$. It appears in the IR spectra as the difference of the splitting of the lower and upper J levels involved in the respective transition. The observed splitting is largest for the Π–Π subband, where it scales with $J(J+1)$. It is much smaller for

TABLE II. Rotational constants (in cm^{-1}) obtained for D$_2$–DCO$^+$ by fitting spectral line positions[a] of the ν_1 band to a Watson A-type Hamiltonian.

D$_2$–DCO$^+$	Σ–Σ	Π–Π	Δ–Δ	Σ–Σ/Π–Π
B''		0.30321(4)		0.30330(5)
C''		0.29915(8)		0.29927(5)
$\bar{B}''$	0.30128(4)	0.30118(4)	0.30161(6)	0.30129(4)
$D_J'' \times 10^6$	1.6 (fixed)	1.6(3.3)	1.5(1.0)	1.57(4)
$D_{JK}'' \times 10^4$				1.4(5)
B'		0.30374(5)		0.30384(5)
C'		0.29959(7)		0.29971(5)
$\bar{B}'$	0.30179(4)	0.30167(4)	0.30080(6)	0.30178(4)
$D_J' \times 10^6$	1.6 (fixed)	1.5(3.0)	3.2(9.0)	1.58(4)
$D_{JK}' \times 10^4$				1.3(5)
$\Delta A = A'' - A'$		1.3105(4)	1.3003(1)	1.3240(4)
ν_0	2923.2956(11)	2921.9733(4)[b]	2918.0887(4)[b]	2923.2968(4)
R branch	$R(0)$–$R(28)$	$R(1)$–$R(29)$	$R(2)$–$R(10)$	
P branch	$P(1)$–$P(29)$	$P(2)$–$P(27)$	$P(3)$–$P(10)$	
Q branch		2921.97(2)	2918.08(2)	
used lines	58	108	36	166
rms$\times 10^3$	3.4	4.1	2.4	4.2

[a]Available from the authors upon request.
[b]Subband origin is calculated from $\nu_0 - K \times \Delta A$.

$K_a > 1$ manifolds and consequently not resolved in the present study for the Δ–Δ band of D$_2$–DCO$^+$.

The measured transition frequencies were fitted to a Watson A-type Hamiltonian[20] including centrifugal distortion constants D_J and D_{JK}. The resulting parameters are compiled in Tables I and II. Each subband was fitted separately, and a global fit including the lines of the Σ–Σ and Π–Π subbands was conducted as well. Inclusion of Δ–Δ transitions for D$_2$–DCO$^+$ drastically increased the residual standard deviation, a first indication of the nonrigidity of the complex.

The rotational constants obtained from the fit cannot be directly converted into physically meaningful equilibrium structures. The *ab initio* geometry[10] of H$_2$–HCO$^+$ (D$_2$–DCO$^+$) corresponds to an asymmetry $B - C$ of 0.0042 cm^{-1} (0.0032 cm^{-1}) in comparison to the significantly higher values of 0.0063 cm^{-1} (0.0040 cm^{-1}) extracted from the global fit to the experimental data. It is impossible to find a reasonable structure which simultaneously matches the ground state $\bar{B}$ and $B - C$ values of H$_2$–HCO$^+$. For example, fixing the HCO$^+$ monomer structure at the recommended values[21] ($r_{CH} = 1.097$ Å, $r_{CO} = 1.105$ Å) and varying the intramolecular H$_2$ bond length together with the intermolecular separation in the T-shaped configuration leads to an intermolecular bond length of 1.84 Å, somewhat larger than the *ab initio* value[10] of 1.74 Å, and to a large and unrealistic increase of the H$_2$ bond length from 0.74 Å in the monomer[18] to 0.95 Å in the complex. In addition, no structure could be found that simultaneously reproduces the $\bar{B}$ and $B - C$ constants of both H$_2$–HCO$^+$ and D$_2$–DCO$^+$. These observations are again interpreted as evidence[14] for the nonrigidity of the complex which is partly accounted for in Sec. III B.

Though the rotational constants are influenced by the internal rotation dynamics, most sensitively the asymmetry $B - C$, they can be used to estimate some properties of the complex in a qualitative way. In general, the constants B and C (and thus also $\bar{B}$) increase upon vibrational excitation, i.e., the interaction in the upper state is stronger, leading to a shorter intermolecular bond. The evaluation of intermolecular separations via a pseudodiatomic approach,[22] assuming undistorted monomers, resulted in slightly different values for H$_2$–HCO$^+$ and D$_2$–DCO$^+$ in both vibrational states. The larger value for H$_2$–HCO$^+$ ($R_{H-H_2} = 1.84$ Å for $v_1 = 0$) compared to D$_2$–DCO$^+$ ($R_{D-D_2} = 1.81$ Å for $v_1 = 0$) is due to larger zero-point motions in the former complex. Both values are also larger than the *ab initio* R_e distance of 1.744 Å. Again, zero-point effects and the significant anharmonicity of the intermolecular stretching motion may at least partly account for this discrepancy. The increase in bond strength upon vibrational excitation is indicated by the decrease of the intermolecular separations of 0.008 and 0.005 Å for H$_2$–HCO$^+$ and D$_2$–DCO$^+$, respectively. The intermolecular radial force constant can roughly be estimated as 10 N/m, again by applying a pseudodiatomic approach.[22]

B. Hindered rotor analysis

The anomalously large asymmetry splitting obtained from the semirigid rotor analysis can be attributed to the hindered rotation of the hydrogen molecule. In order to model this internal motion, a simple atom–diatom hindered rotor Hamiltonian is employed which has been described in detail elsewhere.[14,23,24] The model treats the formyl ion as a point mass. In addition, the radial dependence of the intermolecular potential is neglected.

The model Hamiltonian can be written in space-fixed coordinates as

$$\hat{H} = b\hat{\mathbf{j}}^2 + \bar{B}\hat{\mathbf{l}}^2 + V(\theta), \tag{1}$$

where $\bar{B}\hat{\mathbf{l}}^2$ describes the end-over-end rotation of the atom–diatom complex and $b\hat{\mathbf{j}}^2$ the internal rotation of the diatom. The latter motion is hindered by the intermolecular angular potential $V(\theta)$ which is expanded in a sum of Legendre polynomials

$$V(\theta) = \sum_\lambda V_\lambda P_\lambda(\cos \theta), \tag{2}$$

where θ is the angle between the diatom axis and the intermolecular axis. The Hamilton matrix is diagonalized using basis functions of the form

$$\psi_{jl}^{JM} = \sum_{m_j m_l} \langle jlm_jm_l|JM\rangle Y_{jm_j}Y_{lm_l}. \tag{3}$$

$\hat{\mathbf{J}} = \hat{\mathbf{j}} + \hat{\mathbf{l}}$ describes the total angular momentum (with projection M onto the space-fixed z axis), and $Y_{jm_j}Y_{lm_l}$ are the products of spherical harmonics related to the internal and end-over-end rotations, respectively.

The ψ_{jl}^{JM} are eigenfunctions of the operators $\hat{\mathbf{j}}^2$, $\hat{\mathbf{l}}^2$, $\hat{\mathbf{J}}^2$, and $\hat{\mathbf{J}}_z$. Therefore j, l, J, and M are good quantum numbers in the limit of free internal rotation. The anisotropic part of the potential mixes states with the same J and parity $p' = (-)^{j+1}$, but different j and l. The symmetry of the homonuclear diatom causes terms with odd λ in the $V(\theta)$ expansion (2) to be zero. Thus, only even (or odd) j states interact with each other through $V(\theta)$, corresponding to *ortho* and *para* modifications of the complex. Matrix elements of the space-fixed Hamiltonian (1) with the basis functions (3) are given elsewhere.[23,24] A correlation diagram which illustrates the behavior of energy levels on transformation from a rigid asymmetric top to a free internal rotor by decreasing the potential barrier may be found in Ref. 23. For a T-shaped complex ($V_2 < 0$) and a potential that is dominated by the V_2 term, the effect of decreasing the potential barrier on the semirigid asymmetric top energy levels is to increase the Π state asymmetry splittings and to shift the energies of the various K_a origins. Both observations can be used to infer details of the hindering potential $V(\theta)$ from the experimental spectrum.

For the calculations the parameters presented in Table III were used. The $\bar{B}$ values were taken from the experimental data (Tables I and II). The b values were estimated from the *ab initio* structure of the hydrogen molecule in the T-shaped

TABLE III. Parameters (in cm^{-1}) used for the matrix diagonalization described in Sec. III B.

	H$_2$–HCO$^+$ $v_1=0$	H$_2$–HCO$^+$ $v_1=1$	D$_2$–DCO$^+$ $v_1=0$	D$_2$–DCO$^+$ $v_1=1$
$\bar{B}$	0.4863	0.4876	0.3013	0.3018
b	58.247	55.185	29.350	28.271
V_2	818		818	
V_4	−118		−118	

minimum geometry of the complex[10] ($r_e = 0.751$ Å) and the known α_e parameters of free molecular hydrogen (3.062 and 1.079 cm^{-1} for H$_2$ and D$_2$, respectively[18]). A basis set containing functions up to $j_{max}=13$ and $l_{max}=J+j_{max}$ was sufficient to converge the eigenvalues for J up to 36 to better than 0.001 cm^{-1} for the lowest Σ, Π, and Δ manifolds in both vibrational states. The expansion of the potential was truncated at $\lambda=4$, and V_0 was arbitrarily set to zero. Figure 3 shows the potential for the vibrationless state and the range of calculated energy levels of H$_2$–HCO$^+$ and D$_2$–DCO$^+$ probed by the experiment.

Three types of experimental data may be compared with the simulations: (i) observed transition splittings in the P and R branches of the respective Π–Π transitions which arise from the difference in the asymmetry splittings of a ground state J level and an excited state $J\pm1$ level; (ii) relative shifts of the Δ–Δ and Π–Π transition origins with respect to those of the Σ–Σ bands; (iii) differences of the splittings of a Π state J and $J+2$ level of the same vibrational state which can be extracted by forming ''combination differences.'' In principle, the combination differences should allow for the determination of the V_2 and V_4 potential parameters for each
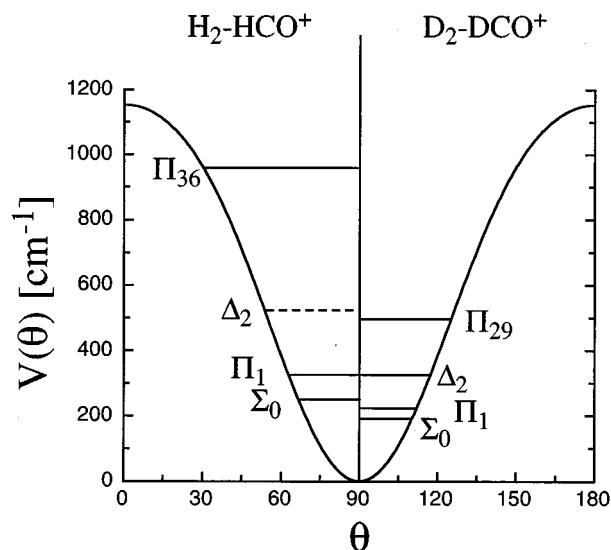

FIG. 3. One-dimensional potential to model the hindered H$_2$ (D$_2$) rotation in H$_2$–HCO$^+$ (D$_2$–DCO$^+$) in the vibrational ground state ($V_2''=818$ cm^{-1}, $V_4''=-118$ cm^{-1}). Indicated are the calculated positions of the lowest lying K_J states as well as the highest levels observed in the experiment for H$_2$–HCO$^+$ (left) and D$_2$–DCO$^+$ (right), respectively. Splittings of the Π_J levels are not shown.

vibrational state separately. The quality of the data is, however, not sufficient to provide them with the required accuracy. Hence, it was decided to consider all three types of data (i–iii) for the simulations, which gave harder restrictions for the potential parameters. As expected, the relative shifts of the origins are most sensitive to changes in the shape of the potential induced by vibrational excitation.

For the lower state, the potential obtained from the *ab initio* calculations[10] was employed: V_2'' and V_4'' were taken as 818 and -118 cm^{-1}, giving rise to a barrier $V_b'' = \frac{3}{2} V_2'' + \frac{5}{8} V_4'' = 1153$ cm^{-1} (Fig. 3). This potential is compatible with the experimental lower state combination differences. The corresponding upper state parameters, V_2' and V_4', were then varied to simultaneously fit the experimentally observed Π–Π transition splittings, the measured relative origin shifts, and the upper state combination differences for both complexes. It was not possible to find an upper state potential parameter set that simultaneously minimizes the differences between experimental and simulated transition splittings and the origin shifts. Fits to the transition splittings alone resulted in $V_2' = 912 \pm 10$ cm^{-1}, $V_4' = -91 \pm 11$ cm^{-1}, and $V_b' = 1311 \pm 22$ cm^{-1}, where V_2' and V_4' are linearly correlated (e.g., $V_2' = 922$ cm^{-1} corresponds to $V_4' = -80$ cm^{-1}, and $V_2' = 902$ cm^{-1} to $V_4' = -102$ cm^{-1}). Fitting only the origin shifts yielded $V_2' = 918 \pm 14$ cm^{-1}, $V_4' = -72 \pm 14$ cm^{-1}, and $V_b' = 1332 \pm 30$ cm^{-1}. Bracketing both intervals for V_b' gives an estimated barrier height of 1325 ± 36 cm^{-1}, which corresponds to an increase of 172 ± 36 cm^{-1} ($\approx 15\%$) upon vibrational excitation. For the presented sets of V_2 and V_4 parameters, the calculated origin shifts, transition splittings, as well as the combination differences showed deviations from the experimentally determined values of less than the laser bandwidth of 0.02 cm^{-1}.

Another criterion for judging the degree of the rigidity of the H$_2$–HCO$^+$ complex along the internal H$_2$ rotation coordinate is provided by the frequency of the intermolecular in-plane bending motion of the H$_2$ unit (ν_8). The *ab initio* calculations predict a harmonic frequency of 608 cm^{-1} for this vibration.[10] In the limit of a free internal rotor, the ground and first excited bending states correspond to the lowest Σ states with rotational quantum numbers (JKjl) $=(0000)$ and (0011). They are separated by approximately $2b$ which amounts to ≈ 120 cm^{-1} in the case of the H$_2$ containing complex. From the hindered rotor simulations utilizing the $v_1=0$ potential, a spacing of 491 cm^{-1} is obtained, which is closer to the value of the rigid harmonic oscillator than that of the free internal rotor. This result is expected because the barrier of ≈ 1150 cm^{-1} is much larger than the internal rotor constant of ≈ 60 cm^{-1}.

Now, several deficiencies of the employed hindered rotor Hamiltonian will be discussed. The one-dimensional model neglects couplings of the internal H$_2$ rotation to other degrees of freedom. As can be seen from Fig. 3, the calculated energy levels of H$_2$–HCO$^+$ and D$_2$–DCO$^+$ probed by the experiment cover almost the entire potential. Consequently, the effects of angular–radial couplings may be important because the intermolecular equilibrium separation depends[10] on the angle θ. In addition, centrifugal distortion

effects may become significant for high J levels. While the origin shifts ($J=0$) are sensitive to the lower part of the potential, the transition splittings measured up to high J levels also probe the upper part. This may explain why within the simple model the origin shifts and the transition splittings cannot be fitted best with the same set of potential parameters. The neglect of the internal rotation of HCO$^+$ is probably a fair approximation because the rotational constant of HCO$^+$, $b_{\text{HCO}^+} \approx 1.5$ cm^{-1}, is significantly lower than the barrier for this internal rotation,[10] $V_b \approx 1300$ cm^{-1}. As a further approximation, the potential $V(\theta)$ in (1) was assumed to be identical for H$_2$–HCO$^+$ and D$_2$–DCO$^+$. However, $V(\theta)$ is a potential averaged over other degrees of freedom, including the intramolecular H$_2$ and CH bond lengths as well as the intermolecular separation. Vibrational averaging of the hindering potential over these coordinates will lead to slightly different potentials for the protonated and the deuterated complex. Finally, the increase in the radial binding energy induced by the ν_1 vibrational excitation was assumed to be the same for Σ, Π, and Δ states. Only under this condition, the experimental relative origin shifts can be compared with the simulated ones. In view of the apparently different binding energies of the complex in the various K_a states (see below), the validity of this approximation may be questionable.

IV. FURTHER DISCUSSION

A. Barrier for H$_2$ internal rotation

The barrier for the internal rotation of the H$_2$ molecule arises from the anisotropy of the intermolecular potential. The considerably higher proton affinity of CO (594 kJ/mol)[25] compared to H$_2$ (423 kJ/mol)[25] implies that the complex can essentially be considered as an H$_2$ molecule associated with a slightly distorted HCO$^+$ ion. To estimate the anisotropy of the long-range part of the interaction, the potential can therefore be approximated by the leading electrostatic and induction terms arising from the monomer properties, namely, the interaction between the positive charge of the HCO$^+$ ion with the quadrupole moment and the polarizability of the H$_2$ molecule:

$$V_{\text{lr}}(R,\theta) = \frac{Q\Theta}{8\pi\epsilon_0 R^3}(3\cos^2\theta - 1)$$
$$-\frac{1}{2}\frac{Q^2(\alpha_\parallel \cos^2\theta + \alpha_\perp \sin^2\theta)}{4\pi\epsilon_0 R^4}. \quad (4)$$

Here, Q is the ion charge, Θ the quadrupole moment of H$_2$ ($+2.12 \times 10^{-40}$ Cm^2),[26] R the distance between the H$_2$ center of mass and the ionic charge, and $\alpha_\perp$ and $\alpha_\parallel$ are the perpendicular and parallel volume polarizabilities of H$_2$ (0.79 and 0.93 Å^3, respectively).[27] The charge–quadrupole interaction plays the dominant role in stabilizing the H$_2$–HCO$^+$ complex in the T-shaped configuration (see also Fig. 2 in Ref. 10).

The contribution to the barrier height (V_b) arising from the long-range potential (4) is given by

$$V_b(R) = V_{lr}(R, \theta = 0°) - V_{lr}(R, \theta = 90°)$$

$$= \frac{3Q\Theta}{8\pi\epsilon_0 R^3} - \frac{Q^2(\alpha_\parallel - \alpha_\perp)}{8\pi\epsilon_0 R^4}. \tag{5}$$

Near the equilibrium distance ($R \approx 2-3$ Å), V_b is dominated by the electrostatic part while the induction term contributes less than 20%. In the vibrational excited state, the quadrupole moment of H$_2$ is $\sim$11% (Refs. 28 and 29) and $\alpha_\parallel - \alpha_\perp$ is $\sim$23% (Refs. 30 and 31) larger than in the ground state, leading to a net increase in the barrier height of approximately 9%. The slight decrease of the intermolecular bond length upon vibrational excitation increases the barrier by less than 1%.

A further contribution to the barrier height may arise from the short-range repulsion. The relative magnitude of this effect is difficult to estimate. However, this contribution will also slightly increase upon vibrational excitation of the H$_2$ stretch, because steric hindrance will be enhanced due to the shorter intermolecular bond and the simultaneously longer H$_2$ bond. The hindered rotor simulations described in Sec. III B gave an increase in the barrier height of roughly 15% upon excitation, suggesting that the dominant contribution to the barrier comes from the electrostatic anisotropic terms rather than from the repulsive interaction. It is noted that for NH$_4^+$–Rg ionic complexes the angular potential anisotropy for fixed intermolecular separations is also controlled by long-range interactions (in this case by induction and dispersion forces).[32,33]

The barrier for internal H$_2$ rotation in H$_2$–HCO$^+$ may be compared with respective barriers in complexes where molecular hydrogen is associated with other neutral or ionic species. Due to the large rotational constant of H$_2$ (60 cm^{-1}) large barriers are necessary to effectively quench this internal motion. The best characterized three-dimensional potential energy surface of an atom–diatom system is probably that of H$_2$–Ar.[34,35] The attractive interaction in this system with linear equilibrium structure is governed by dispersion energy. The barrier for internal rotation is less than 10 cm^{-1}, i.e., significantly smaller than the rotational constant of H$_2$ ($\approx$60 cm^{-1}) which is of the order of the binding energy of the complex, $D_e \approx 50-60$ cm^{-1}. The zero-point energy level lies above the barrier, resulting in an almost free internal rotation of H$_2$. Similarly, in the even weaker bound (H$_2$)$_2$ dimer ($D_0 \approx 3$ cm^{-1}), the hindering potential terms are much smaller than the diatom rotational constant.[36] Spectroscopic studies on H$_2$–HF revealed that this complex has a T-shaped minimum geometry,[23,37] as is expected from the long-range dipole–quadrupole interaction. The internal rotor constant is in this case smaller than the barrier of about 230 cm^{-1} for H$_2$ rotation and also below the binding energy of $\approx$150 cm^{-1}. Though the angular anisotropy is large enough to lock the complex in the T-shaped geometry, the effects of zero-point excursions on the spectrum of the HF vibration cannot be neglected.

It appears that, compared to the neutral H$_2$ containing systems, the charge in the H$_2$–HCO$^+$ ionic complex implies not only a stronger and thus shorter intermolecular bond, due
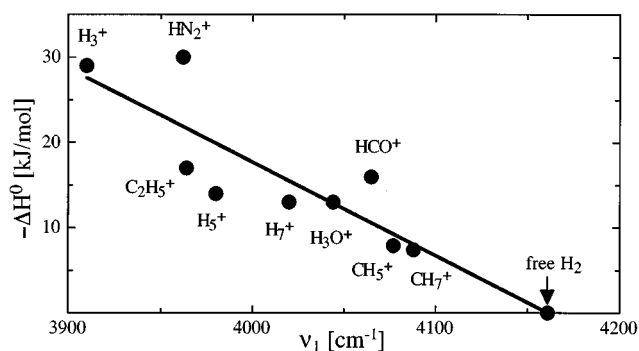

FIG. 4. Correlation between the ν_1 frequencies (H$_2$ stretch) and binding energies of various H$_2$–M^+ complexes. The values are taken from Table IV. For comparison, the frequency of the uncomplexed H$_2$ monomer ($\Delta H^0 = 0$) is included as well. The line represents a linear fit to the data points.

to additional electrostatic and induction forces, but also causes a larger angular anisotropy in the intermolecular potential, which mainly arises from the charge–quadrupole interaction. Though the barrier of $V_b \approx 10^3$ cm^{-1} is significantly larger than the H$_2$ rotational constant, the effects of the nonrigidity are clearly visible in the spectrum of the complex. *Ab initio* calculations predict for the related T-shaped H$_2$–H$_3^+$ complex ($D_e \approx 2800$ cm^{-1}) a barrier of about 2150 cm^{-1} for the internal H$_2$ rotation via the planar transition state with the H$_2$ molecule oriented along the intermolecular bond.[38] Both the binding energy and the barrier for H$_2$ rotation are larger in this complex compared to H$_2$–HCO$^+$, suggesting a correlation between the intermolecular bond strength and the internal rotation barrier height in similar complexes composed of H$_2$ and molecular ions.

B. Frequency shift and binding energy

The ν_1 fundamental is dipole forbidden for the free hydrogen molecule; however, complexation with the formyl ion induces a nonvanishing transition moment for this mode along the intermolecular axis. A further effect of clustering is the reduction of the frequency of this vibration by -96.4 cm^{-1} from 4161.2 cm^{-1} in the free H$_2$ molecule[39] down to 4064.8 cm^{-1} in the H$_2$–HCO$^+$ complex. For the deuterated complex, the corresponding frequency drops upon complexation by -70.3 cm^{-1} from 2993.6 (Ref. 39) to 2923.3 cm^{-1}. The observed redshifts directly reflect the stronger intermolecular bond in the vibrational excited state, mainly arising from the increased electrostatic and polarization interaction. As expected, the magnitude of the ν_1 frequency shifts of 2.3% in the H$_2$–HCO$^+$/D$_2$–DCO$^+$ ionic complexes is significantly larger than that of related neutral species. For example, in H$_2$–Rg systems (Rg=Ar, Kr, Xe) the redshifts[40] are less than 3 cm^{-1} ($\approx$0.07%).

As has been suggested previously,[41] the reduction of the ν_1 frequency in complexes of H$_2$ with molecular ions (M^+) can be correlated with their intermolecular bond strengths. Figure 4 and Table IV compare the ν_1 frequencies with the binding energies for a number of H$_2$–M^+ complexes, and

TABLE IV. H$_2$ stretching frequencies and binding energies for selected H$_2$–M^+ complexes.

M^+	$-\Delta H^0(\mathrm{H_2}-M^+)$ (kJ/mol)	ν_1 (cm^{-1})
H$_3$O$^+$	≈ 13[a]	4046[a]
HCO$^+$	16[b]	4065
HN$_2^+$	30[c]	3962[g]
CH$_5^+$	7.9[d]	4077[h]
H$_2$–CH$_5^+$	7.4[d]	4088[h]
C$_2$H$_5^+$	17[e]	3964[i]
H$_3^+$	29[f]	3910[j]
H$_5^+$	14[f]	3980[j]
H$_7^+$	13[f]	4020[j]

[a]Ref. 41. [f]Ref. 53.
[b]Ref. 49. [g]Ref. 54.
[c]Ref. 50. [h]Ref. 55.
[d]Ref. 51. [i]Ref. 56.
[e]Ref. 52. [j]Ref. 57.

indeed a systematic trend is found. Complexes with stronger intermolecular bonds feature larger ν_1 redshifts. A connection between the ν_1 frequency and the electrostatic interaction energy in H$_2$–M^+ complexes has been derived by Poll and Hunt.[42] In a perturbation approach, they calculated the Stark shifts of the H$_2$ and D$_2$ ν_1 frequencies induced by the presence of a point charge located at a distance R away from the molecular center of mass. The potential given in (4) was added to the zero-order Hamiltonian of molecular hydrogen as the perturbation term. The charge-induced redshifts calculated in Ref. 42 for selected R values are plotted in Fig. 5 against the electrostatic and induction energy obtained from Eq. (4), and a nearly linear dependence between these two quantities is found. For $R \approx 2.65$ Å, the ν_1 redshifts of H$_2$ and D$_2$ are calculated to be 97 and 70 cm^{-1}, i.e., quite close to the shifts of -96.4 and -70.3 cm^{-1} measured for H$_2$–HCO$^+$ and D$_2$–DCO$^+$, respectively. Taking into account the calculated *ab initio* geometry,[10] this implies that according to this model the effective ''point charge'' in H$_2$–HCO$^+$ is located on the CH bond some 0.2 Å away from the C atom. For comparison, the Mulliken analysis[43] predicts the center of charge to lie about 0.4 Å away from carbon.
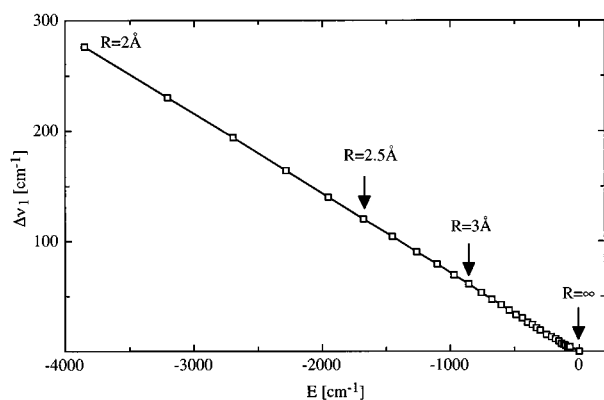

FIG. 5. The redshift of the fundamental frequency of H$_2$ induced by a point charge at certain distances R away from the molecular center of mass vs the interaction energy (see text and Ref. 42 for details).

This disagreement arises partly from the fact that the extension of the charge distribution in the molecular ion and repulsive contributions to the intermolecular bond have been neglected. In addition, the formation of the complex may be accompanied by some amount of electron density donation from the H$_2$ σ bond into the intermolecular bond, thus weakening the H$_2$ bond and strengthening the intermolecular bond due to covalent-type bonding. Though this effect may be small for H$_2$–HCO$^+$, it will be significant for complexes of H$_2$ with protonated ions MH$^+$, where M has a similar or even smaller proton affinity as H$_2$, for example, $M =$ H$_2$, Ar, or Kr.

Analysis of the relative intensities of the Π–Π and Σ–Σ subbands reveals that the former is somewhat stronger than expected for both H$_2$–HCO$^+$ and D$_2$–DCO$^+$. Assuming that the complexes are formed under high temperature conditions and cooled down by subsequent collisions, the intensity ratio should be determined by the nuclear spin weights of $K =$ even and $K =$ odd states, i.e., 1:3 (2:1) for the Π–Π and Σ–Σ subbands of H$_2$–HCO$^+$ (D$_2$–DCO$^+$). In the low temperature limit, the K-type doubling of the Π state has to be taken into account, leading to a corresponding ratio of 1:6 (2:2). The experimental spectra show, however, relative intensities of approximately 1:8 (2:5). In the D$_2$–DCO$^+$ spectrum, the lower population of the Σ state can only partly be explained by incomplete collisional cooling of the Δ state population into the Σ state. Another reason for the enhanced Π state population for both isotopic complexes may arise from the higher binding energy of Π state complexes leading to an enhanced production in the ion source. The probability for the hydrogen molecule to sample the energetically higher lying linear configuration is larger in the Σ state compared to the Π state.[10] The resulting weaker and longer intermolecular bond in the Σ state is also indicated by the respective rotational constants (see above). Finally, it is noted that a similar effect was previously observed in the IR spectra of the related complexes H$_2$–HF and D$_2$–HF (Refs. 23 and 37).

C. Rotational distribution

To estimate the rotational temperature describing the J level population, Boltzmann plots are created for the Σ–Σ and Π–Π bands of D$_2$–DCO$^+$ and the Π–Π band of H$_2$–HCO$^+$ (the latter one is shown in Fig. 6). The Σ–Σ band of H$_2$–HCO$^+$ and the Δ–Δ band of D$_2$–DCO$^+$ were too weak to extract reliable information about their rotational distributions. The absorption intensities were approximated by those of a rigid symmetric top,[19]

$$I = \mathrm{const} \times A \times \nu \times g \times e^{-(F/kT)}, \qquad (6)$$

which include the Hönl–London factor A, the transition frequency ν, the respective degeneracy factors g, and the exponential Boltzmann term. In addition, it is assumed that variations in the photodissociation cross section are solely arising from the absorption cross sections, i.e., the line intensities are not affected by differing predissociation rates of the upper state levels. The integrated intensities of the Π–Π transition doublets were added for each J, and the normalized
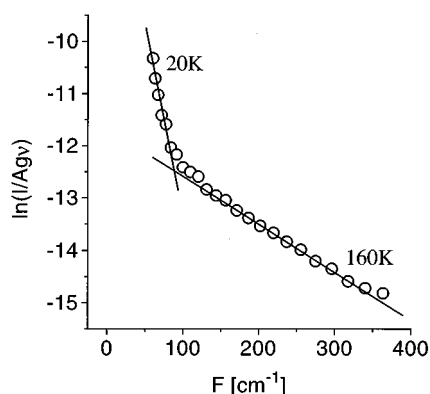
FIG. 6. Boltzmann plot for the Π–Π band of H_2–HCO^+.

intensities ($I/A\nu g$) were averaged for P and R branch lines starting from the same lower state. As can be seen from Fig. 6, the distributions cannot be described by a single temperature. As is typical for jet expansions of neutral[44,45] and ionic species,[46–48] the population of higher J levels is larger than predicted by the Boltzmann distribution fitted to the population of the low J levels. For the investigated subbands of H_2–HCO^+ and D_2–DCO^+, the low J level population can be characterized by a temperature of approximately 20 K, whereas for the higher J levels a temperature of the order of 100–200 K is more appropriate.

D. Lifetimes

In the previous study,[10] the lifetimes of the ν_1 (H_2 stretch) and ν_2 (CH stretch) vibrations of H_2–HCO^+ have been estimated from the observed linewidths to be ≈ 90 ps and < 1 ps, respectively. In the present work, the spectra of both transitions were remeasured at significantly lower laser power, thus avoiding the effects of power broadening. The rotational ν_1 band lines of both H_2–HCO^+ and D_2–DCO^+ possess laser limited linewidths (0.02 cm^{-1}) corresponding to a lower limit of 250 ps for the upper state lifetime. For the ν_2 vibrational band of H_2–HCO^+, however, no rotational substructure could be resolved even for the lowest laser power used, confirming the previous conclusion of rapid predissociation.[10] The substantially longer lifetime of the higher frequency ν_1 vibrational level implies that predissociation in this complex is a highly nonstatistical process. As is discussed in detail elsewhere,[10] this behavior may be rationalized in terms of different efficiencies for the coupling of these two intramolecular fundamentals to the intermolecular degrees of freedom.

V. CONCLUSIONS

The analysis of the rotationally resolved ν_1 band spectra of H_2–HCO^+ and D_2–DCO^+ revealed spectral fingerprints of their nonrigidity. Barriers for the hindered internal rotation of molecular hydrogen could be estimated to be of the order of 1150 cm^{-1} by applying a simple one-dimensional hindered rotor Hamiltonian. It appears that the origin of the barrier for this internal motion mainly arises from the angu-

lar anisotropy of the long-range intermolecular forces which in this particular case is dominated by the charge–quadrupole interaction. Thus, the approximate 15% increase of the barrier upon ν_1 excitation can be rationalized by the larger quadrupole moment of molecular hydrogen in the vibrational excited state. A systematic comparison of complexes composed of H_2 and molecular ions suggests a correlation between their complexation induced ν_1 redshifts and their intermolecular bond strengths.

[1] C. S. Yeh, J. S. Pilgrim, K. F. Willey, D. L. Robbins, and M. A. Duncan, Int. Rev. Phys. Chem. **13**, 231 (1994).

[2] M. W. Crofton, J. M. Price, and Y. T. Lee, in *Clusters of Atoms and Molecules II* (Springer-Verlag, Berlin, 1994), Vol. 56, p. 44.

[3] E. J. Bieske and J. P. Maier, Chem. Rev. **93**, 2603 (1993).

[4] J. M. Lisy, in *Cluster Ions* (Wiley, New York, 1993), p. 217.

[5] A. Carrington, A. M. Shaw, and S. M. Taylor, J. Chem. Soc. Faraday Trans. **91**, 3725 (1995).

[6] M. S. Johnson, K. T. Kuwata, C. K. Wong, and M. Okumura, Chem. Phys. Lett. **260**, 551 (1996).

[7] D. J. Nesbitt, Chem. Rev. **88**, 843 (1988).

[8] K. R. Leopold, G. T. Fraser, S. E. Novick, and W. Klemperer, Chem. Rev. **94**, 1807 (1994).

[9] K. Müller-Dethlefs, O. Dopfer, and T. G. Wright, Chem. Rev. **94**, 1845 (1994).

[10] E. J. Bieske, S. A. Nizkorodov, F. R. Bennett, and J. P. Maier, J. Chem. Phys. **102**, 5152 (1995).

[11] S. A. Nizkorodov, J. P. Maier, and E. J. Bieske, J. Chem. Phys. **103**, 1297 (1995).

[12] S. A. Nizkorodov, O. Dopfer, M. Meuwly, J. P. Maier, and E. J. Bieske, J. Chem. Phys. **105**, 1770 (1996).

[13] S. A. Nizkorodov, O. Dopfer, T. Ruchti, M. Meuwly, J. P. Maier, and E. J. Bieske, J. Phys. Chem. **99**, 17118 (1995).

[14] D. J. Nesbitt and R. Naaman, J. Chem. Phys. **91**, 3801 (1989).

[15] E. J. Bieske, J. Chem. Soc. Faraday Trans. **91**, 1 (1995).

[16] G. Guelachvili and K. N. Rao, *Handbook of Infrared Standards* (Academic, London, 1993).

[17] S. M. Beck, M. G. Liverman, D. L. Monts, and R. E. Smalley, J. Chem. Phys. **70**, 232 (1979).

[18] K. P. Huber and G. Herzberg, *Molecular Spectra and Molecular Structure* (Van Nostrand Reinhold, New York, 1979), Vol. IV.

[19] G. Herzberg, *Molecular Spectra and Molecular Structure* (Krieger, Malabar, FL, 1991), Vol. II.

[20] J. K. G. Watson, in *Vibrational Spectra and Structure* (Elsevier, New York, 1977).

[21] R. C. Woods, Philos. Trans. R. Soc. London, Sec. A **324**, 141 (1988).

[22] D. C. Millen, Can. J. Chem. **63**, 1477 (1985).

[23] C. M. Lovejoy, D. D. Nelson, and D. J. Nesbitt, J. Chem. Phys. **87**, 5621 (1987).

[24] J. M. Hutson, in *Advance in Molecular Dynamics and Collision Dynamics* (JAI P, Greenwich, CT, 1991), Vol. 1, p. 1.

[25] S. G. Lias, J. E. Bartmess, J. F. Liebman, J. L. Holmes, R. D. Levin, and W. G. Mallard, J. Phys. Chem. Ref. Data **17**, (1988).

[26] W. H. Flygare and R. C. Benson, Mol. Phys. **20**, 225 (1971).

[27] C. J. F. Boettcher and P. Borderwijk, *Theory of Electric Polarization* (Elsevier, Amsterdam, 1978).

[28] D. E. Stogryn and A. P. Stogryn, Mol. Phys. **11**, 371 (1966).

[29] L. M. Wolniewicz, J. Chem. Phys. **45**, 515 (1966).

[30] R. J. Le Roy and C. Schwart, Chemical Physics Research Report No. CP-301, University of Waterloo, 1987.

[31] C. Schwartz and R. J. LeRoy, J. Mol. Spectrosc. **121**, 420 (1987).
[32] M. Meuwly, S. A. Nizkorodov, E. J. Bieske, J. P. Maier, and O. Dopfer, Chem. Phys. Lett. **270**, 252 (1997).
[33] J. P. Read and A. D. Buckingham, Chem. Phys. Lett. **270**, 245 (1997).
[34] C. Bissonnette, C. Chuaqui, K. G. Crowell, R. J. Le Roy, R. J. Wheatley, and W. J. Meath, J. Chem. Phys. **105**, 2639 (1996).
[35] A. R. W. McKellar, J. Chem. Phys. **105**, 2628 (1996).
[36] A. R. W. McKellar, J. Chem. Phys. **92**, 3261 (1990).
[37] C. M. Lovejoy, D. D. Nelson, and D. J. Nesbitt, J. Chem. Phys. **89**, 7180 (1988).
[38] Y. Yamaguchi, J. F. Gaw, R. B. Remmington, and H. F. Schaefer III, J. Chem. Phys. **86**, 5072 (1987).
[39] A. R. W. McKellar, Faraday Discuss. Chem. Soc. **73**, 89 (1982).
[40] A. R. W. McKellar and H. L. Welsh, J. Chem. Phys. **55**, 595 (1971).
[41] M. Okumura, L. I. Yeh, J. D. Myers, and Y. T. Lee, J. Phys. Chem. **94**, 3416 (1990).
[42] J. D. Poll and J. L. Hunt, Can. J. Phys. **63**, 84 (1985).
[43] B. Weis and K. Yamashita, J. Chem. Phys. **99**, 9512 (1993).
[44] T. E. Gough and R. E. Miller, J. Chem. Phys. **78**, 4486 (1983).

[45] D. Bassi, A. Boschetti, S. Marchetti, G. Scoles, and M. Zen, J. Chem. Phys. **74**, 2221 (1981).
[46] T. Ruchti, A. Rohrbacher, T. Speck, J. P. Connelly, E. J. Bieske, and J. P. Maier, Chem. Phys. Lett. **209**, 169 (1996).
[47] D. T. Anderson, S. Davis, T. S. Zwier, and D. J. Nesbitt, Chem. Phys. Lett. **258**, 207 (1996).
[48] Y. Xu, M. Fukushima, T. Amano, and A. R. W. McKellar, Chem. Phys. Lett. **242**, 126 (1995).
[49] K. Hiraoka and P. Kebarle, J. Chem. Phys. **63**, 1688 (1975).
[50] K. Hiraoka, P. P. Saluja, and P. Kebarle, Can. J. Chem. **57**, 2159 (1979).
[51] K. Hiraoka, I. Kudaka, and S. Yamabe, Chem. Phys. Lett. **184**, 271 (1991).
[52] K. Hiraoka and P. Kebarle, J. Am. Chem. Soc. **98**, 6119 (1976).
[53] K. Hiraoka, J. Chem. Phys. **87**, 4048 (1987).
[54] E. J. Bieske, S. A. Nizkorodov, F. Bennett, and J. P. Maier, Int. J. Mass Spectrom. Ion Process. **150**, 167 (1995).
[55] D. W. Boo and Y. T. Lee, J. Chem. Phys. **103**, 520 (1995).
[56] L. I. Yeh, J. M. Price, and Y. T. Lee, J. Am. Chem. Soc. **111**, 5597 (1989).
[57] M. Okumura, L. I. Yeh, and Y. T. Lee, J. Chem. Phys. **88**, 79 (1988).